DOI:10.11776/j.issn.1000-4939.2025.06.019

应变梯度高阶剪切变形微板的自由振动特性研究

孔维嘉[1,2],张波[1,2],段宇杭[1,2],沈火明[1,2],张旭[1,2]

(1.应用力学与结构安全四川省重点实验室,610031 成都;2.西南交通大学力学与航空航天学院,610031 成都)

摘 要:基于修正的应变梯度理论和精化高阶剪切变形理论,建立了包含 3 个材料尺度参数和 2 个位移场变量的矩形微板自由振动模型,推导了对应的控制微分方程。利用 Navier 法获得了四边简支矩形微板自由振动的解析解。融合 Gauss-Lobatto 求积准则和微分求积准则,构造了一种 4 节点 72 自由度的微分求积有限元,以求解微板在一般边界条件下的自由振动。通过典型数值算例,验证了本研究模型的有效性,探讨了边界条件、材料尺度参数、长宽比、长厚比等对微板振动频率及模态振型的影响。结果表明,矩形微板各阶振动频率和部分模态振型呈现出尺度效应,且其强弱受到边界条件和几何尺寸的影响。

关键词:修正的应变梯度理论;精化高阶剪切变形理论;矩形微板;自由振动;微分求积有限元

中图分类号:TB383;TB34 **文献标志码**:A **文章编号**:1000-4939(2025)06-1397-13

Research on vibration characteristics of strain gradient higher-order shear deformable microplates

KONG Weijia[1,2],ZHANG Bo[1,2],DUAN Yuhang[1,2],SHEN Huoming[1,2],ZHANG Xu[1,2]

(1. Applied Mechanics and Structure Safety Key Laboratory of Sichuan Province,610031 Chengdu,China;
2. School of Mechanics and Aerospace Engineering,Southwest Jiaotong University,610031 Chengdu,China)

Abstract:This paper develops a free vibration model of rectangular microplates including three material length scale parameters and two displacement field variables using the modified strain gradient theory and a refined higher-order shear deformation theory,and presented the related governing differential equations. The analytical vibration frequencies of a four-edge supported rectangular microplate were obtained via the Navier method. Combining the Gauss-Lobatto quadrature and differential quadrature rules,a four-node seventy-two-DOF differential quadrature finite element was constructed to solve the free vibration of rectangular microplates with general boundary conditions. Through typical numerical examples,the effectiveness of the present model was established,and the effects of boundary conditions,material length scale parameters,aspect ratio and length-thickness ratio on the vibration frequencies and mode shapes of rectangular microplates were revealed. The results indicate that the vibration frequencies and some mode shapes of rectangular microplates exhibit significant size effect,and its intensity is associated with the boundary conditions and geometric dimensions.

收稿日期:2023-06-12
基金项目:国家自然科学青年基金资助项目(No. 11602204);四川省自然科学基金资助项目(No. 23NSFSC0849)
通信作者:张波,副教授。E-mail:zhangbo2008@swjtu.edu.cn
引用格式:孔维嘉,张波,段宇杭,等.应变梯度高阶剪切变形微板的自由振动特性研究[J].应用力学学报,2025,42(6):1397-1409.
KONG Weijia,ZHANG Bo,DUAN Yuhang,et al. Research on vibration characteristics of strain gradient higher-order shear deformable microplates[J]. Chinese journal of applied mechanics,2025,42(6):1397-1409.

Key words: modified strain gradient theory; refined higher-order shear deformation theory; rectangular microplate; free vibration; differential quadrature finite element

随着超精密机械加工和半导体技术的迅猛发展,各类微纳米器件不断涌现出来并被应用于航空航天、未来医疗、人工智能、物联网、智慧城市等重要前沿领域。与宏观器件相比,微纳米器件具有体积小、质量轻、成本低、功耗低、可靠性高、易于批量化制造等优点。当器件特征尺寸减小至微纳米量级时,其材料固有力学性能呈现出显著的尺度依赖性[1-4],典型形式包括非局部效应、应变梯度效应和表面效应。经典连续介质力学理论因不包含反映材料微观缺陷的特征长度参数,使其预测结果与微纳米尺度物理事实不符。分子动力学模拟系统内所有原子行为,计算规模庞大,难以求解较大规模或较长时间跨度的问题。鉴于此,研究者开始摒弃经典连续介质力学理论"局部化假设",采用唯象方法构建出表征微纳米尺度效应的非经典连续介质力学理论,如修正的偶应力理论(modified couple stress theory, MCST)[5]、修正的应变梯度理论(modified strain gradient theory, MSGT)[2]以及非局部应变梯度理论(nonlocal strain gradient theory, NSGT)[6]。

过去二十年间,许多学者将 MCST、MSGT 以及 NSGT 与板的各种变形假设相结合以探索微纳米结构静动力学响应新现象和新机理,并取得了丰硕成果。张立民等[7]利用精化高阶剪切变形理论[8]和 MCST 研究了由 Winkler-Pasternak 弹性夹层连接的双层微板系统的面内压缩屈曲行为,推导了各层均为四边简支时系统发生同步/异步屈曲的解析解。马云龙等[9]在 MCST 下建立了静电驱动 Kirchhoff 微板模型,得到了不同于宏观情形的预测结果。王平等[10-12]分别研究了非局部微薄板在磁场及机械载荷作用下磁弹性稳定性问题、应变梯度双层微板在静电力作用下的首次穿越失效问题以及非局部载流纳米板在磁场及机械载荷作用下的随机振动问题,所考虑边界条件均为四边简支。DUAN 等[13-14]结合精化高阶剪切变形理论[8]和 MCST 建立了受面内复合荷载作用的斜微板的屈曲模型,构造了求解相应边值问题的 C^1 型微分求积有限元,呈现了微板屈曲荷载及模态的尺度依赖性。WEI 等[15]在 Kirchhoff-Love 假设和 MCST 下预测了双向功能梯度环形微板轴对称静力弯曲、自由振动以及轴向压缩屈曲行为,借助广义微分求积法求解了 3 类边值问题。KARAMANLI[16]在高阶剪切-法向伸缩变形理论[17]和 MCST 下构建了求解三向功能梯度微板静力弯曲、自由振动以及轴向压缩屈曲的有限元法,其中材料等效性能参数和材料尺度参数沿 3 个方向变化,而孔隙率体积分数仅沿厚度方向变化。MIRSALEHI 等[18]结合 Kirchhoff-Love 假设和 MSGT 提出了分析功能梯度微板振动和屈曲的样条有限元法,揭示了几何尺寸和物理参数对微板临界屈曲载荷和固有频率的影响。TIMOSHIN 等[19]从 Mindlin 剪切变形理论和 MSGT 出发,发展了预测矩形微板非线性受迫振动响应的 C^1 型有限元法。基于精化高阶剪切变形理论[8]和 MSGT,ZHANG 等[17,20]推导了功能梯度圆形/矩形微板静力弯曲、自由振动与面内压缩屈曲的控制微分方程,依次采用微分求积法和 Navier 法求解了简支/固支圆形微板和四边简支矩形微板的 3 类边值问题;THAI 等[21]建立了由六方铍晶体组成的功能梯度各向异性圆形/矩形微板的自由振动模型,发展了求解相应边值问题的等几何分析方法,讨论了几何形状、边界条件、长厚比、梯度指数和材料长度尺度参数等对微板振动频率的影响。KARAMANLI 等[22]在高阶剪切-法向伸缩变形理论[17]和 MCST 下构造了面内位移(u 和 v)、纯弯曲挠度(w_b)、纯剪切挠度(w_s)、法向伸缩挠度(w_z)满足 C^1 连续的四节点有限元,以求解多向功能梯度矩形微板静力弯曲、自由振动和面内压缩屈曲问题。需要指出的是,文献[22]中势能泛函包含 u、v 和 w_z 的二阶偏导数以及 w_b、w_s 的三阶偏导数,这意味着 w_b 和 w_s 需具备 C^2 连续性而非 C^1 连续性。KARAMANLI 等[23]在文献[22]基础上构造了 w_b、w_s 均满足 C^1 过分连续的四节点有限元以及 w_b、w_s 均满足 C^2 弱连续的四节点有限元,并将之应用于预测正弦阶跃荷载和指数爆炸载荷下功能梯度微板瞬态响应。HUNG 等[24]采用等几何分析方法预测了 3 种类型孔隙率分布下多孔泡沫金属微板自由振动和压缩屈曲特性。TANZADEH 等[25]在 NSGT 下发展了一种半解析高阶有线条法,以求解正交各向异性 Kirchhoff 纳米板的屈曲问题,其中挠度场及其一阶、二阶导数采用高阶 Hermitian 形函数来构造,探讨了边界条件、非局部参数、应变梯度参数以及面内加载类型对正交各向异性微板屈曲特性的影响。

CUONG-LE 等[26]在 NSGT 下建立了求解 S 型功能梯度 Mindlin 纳米板静力弯曲、自由振动以及压缩屈曲问题的等几何分析方法,探讨了微板力学特性随材料沿板厚度方向变化、中性层位置、非局部参数、应变梯度参数以及材料梯度指数的变化。

综上所述,目前关于高阶剪切变形微板力学行为尺度效应的研究工作正在不断增加,且出现了一些重要模型,但已有模型主要基于 MCST 和 NSGT 开展,而甚少涉及 MSGT 的情形。在 MSGT 和精化高阶剪切变形理论下,微板势能泛函中涉及到纯弯曲挠度和纯剪切挠度的三阶导数,这将导致模型的控制微分方程显著升阶和高阶边界条件的出现,最终给边值问题求解带来了极大困难。本研究拟在 MSGT 和文献[8]中精化高阶剪切变形理论下,建立微尺度厚板的自由振动模型,构造出相应的微分求积有限元法,探讨振动频率及模态振型随微板边界条件、长厚比、材料尺度参数等因素的变化规律。

1　自由振动模型

在 MSGT 下,各向同性线弹性体的变形能为[2]

$$\Pi_s = \frac{1}{2}\int_V [\varepsilon_{ij}\sigma_{ij} + \gamma_i p_i + \chi_{ij}^{(s)} m_{ij}^{(s)} + \eta_{ijk}^{(1)}\gamma_{ijk}^{(1)}]\,\mathrm{d}V \tag{1}$$

式中:ε_{ij} 是应变张量分量;γ_i 是膨胀梯度张量分量;$\eta_{ijk}^{(1)}$ 是偏斜拉伸梯度张量分量;$\chi_{ij}^{(s)}$ 是曲率张量分量;σ_{ij}、p_i、$\tau_{ijk}^{(1)}$、$m_{ij}^{(s)}$ 依次与 ε_{ij}、γ_i、$\eta_{ijk}^{(1)}$、$\chi_{ij}^{(s)}$ 能量共轭。以上变形度量定义为[2]

$$\varepsilon_{ij} = \frac{1}{2}(u_{i,j} + u_{j,i}),\ \gamma_i = \frac{\partial \varepsilon_{mm}}{\partial x_i},$$

$$\chi_{ij}^{(s)} = \frac{1}{4}\left(\in_{imn}\frac{\partial^2 u_n}{\partial x_m \partial x_j} + \in_{jmn}\frac{\partial^2 u_n}{\partial x_m \partial x_i}\right),$$

$$\eta_{ijk}^{(1)} = \frac{1}{3}\left(\frac{\partial \varepsilon_{jk}}{\partial x_i} + \frac{\partial \varepsilon_{ki}}{\partial x_j} + \frac{\partial \varepsilon_{ij}}{\partial x_k}\right) - \frac{\delta_{ij}}{15}\left(\frac{\partial \varepsilon_{mm}}{\partial x_k} + \frac{\partial \varepsilon_{mk}}{\partial x_m}\right) - \frac{\delta_{jk}}{15}\left(\frac{\partial \varepsilon_{mm}}{\partial x_i} + \frac{\partial \varepsilon_{mi}}{\partial x_m}\right) - \frac{\delta_{ki}}{15}\left(\frac{\partial \varepsilon_{mm}}{\partial x_j} + \frac{\partial \varepsilon_{mj}}{\partial x_m}\right) \tag{2}$$

式中:u_i 为位移分量;δ_{ij} 为 Kronecker 符号;$\in_{imn}$ 为置换符号。

本构方程为

$$\sigma_{ij} = \lambda \varepsilon_{mm}\delta_{ij} + 2G\varepsilon_{ij},\ p_i = 2Gl_0^2\gamma_i,$$
$$\tau_{ijk}^{(1)} = 2Gl_1^2\eta_{ijk}^{(1)},\ m_{ij}^{(s)} = 2Gl_2^2\chi_{ij}^{(s)} \tag{3}$$

式中:l_0、l_1 和 l_2 是材料尺度参数;λ 与 G 依次为第一和第二 Lamé 常数。

图 1 所示矩形微板,长度、宽度、厚度分别为 L_x、L_y、h,材料弹性模量、泊松比、剪切模量、密度分别为 E、ν、G、ρ。笛卡尔直角坐标系 o-xyz 的坐标面 xoy 与微板中面 Ω 重合且原点位于中面左上角。微板的位移场由精化高阶剪切变形理论[8]描述

$$u_z = w_b(x,y,t) + w_s(x,y,t),$$
$$u_x = -zw_{b,x} - \frac{4z^3 w_{s,x}}{3h^2},\ u_y = -zw_{b,y} - \frac{4z^3 w_{s,y}}{3h^2} \tag{4}$$

式中,w_b 和 w_s 分别是中面纯弯曲和纯剪切引起的挠度。

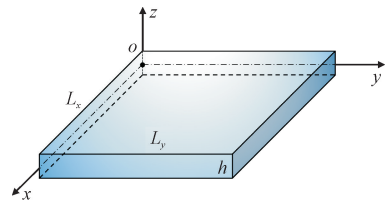

图 1　矩形微板示意图

Fig. 1　Geometry of a rectangular microplate

利用式(2)和式(4)可得微板的应变张量、膨胀梯度张量、偏斜拉伸梯度张量以及旋转梯度张量的非零分量。

$$\varepsilon_{xx} = -zw_{b,xx} - \frac{4z^3 w_{s,xx}}{3h^2},$$
$$\varepsilon_{yy} = -zw_{b,yy} - \frac{4z^3 w_{s,yy}}{3h^2},\ \varepsilon_{xy} = -zw_{b,xy} - \frac{4z^3 w_{s,xy}}{3h^2},$$
$$\varepsilon_{xz} = \left(\frac{1}{2} - \frac{2z^2}{h^2}\right)w_{s,x},\ \varepsilon_{yz} = \left(\frac{1}{2} - \frac{2z^2}{h^2}\right)w_{s,y} \tag{5}$$

$$\gamma_x = -z(w_{b,xxx} + w_{b,xyy}) - \frac{4z^3}{3h^2}(w_{s,xxx} + w_{s,xyy}),$$
$$\gamma_y = -z(w_{b,xxy} + w_{b,yyy}) - \frac{4z^3}{3h^2}(w_{s,xxy} + w_{s,yyy}),$$
$$\gamma_z = -(w_{b,xx} + w_{b,yy}) - \frac{4z^2}{h^2}(w_{s,xx} + w_{s,yy}) \tag{6}$$

$$\eta_{xxx}^{(1)} = \frac{z}{5}(3w_{b,xyy} - 2w_{b,xxx}) + \frac{8zw_{s,x}}{5h^2} + \frac{4z^3}{15h^2}(3w_{s,xyy} - 2w_{s,xxx}),$$
$$\eta_{yxx}^{(1)} = \eta_{xxy}^{(1)} = \eta_{xyx}^{(1)} = \frac{8zw_{s,y}}{15h^2} - \frac{z}{5}(4w_{b,xxy} - w_{b,yyy}) - \frac{4z^3}{15h^2}(4w_{s,xxy} - w_{s,yyy}),$$
$$\eta_{xxz}^{(1)} = \eta_{zxx}^{(1)} = \eta_{xzx}^{(1)} = \frac{1}{15}(w_{b,yy} - 4w_{b,xx} + 4w_{s,xx} - w_{s,yy}) -$$

$$\frac{8z^2}{15h^2}(4w_{s,xx}-w_{s,yy})\,,$$

$$\eta_{yxy}^{(1)}=\eta_{xyy}^{(1)}=\eta_{yyx}^{(1)}=\frac{z}{5}(w_{b,xxx}-4w_{b,xyy})+\frac{4z^3}{15h^2}(w_{s,xxx}-4w_{s,xyy})+\frac{8zw_{s,x}}{15h^2}\,,$$

$$\eta_{zyx}^{(1)}=\eta_{yxz}^{(1)}=\eta_{xzy}^{(1)}=\eta_{xyz}^{(1)}=\eta_{zxy}^{(1)}=\eta_{yzx}^{(1)}=\frac{1}{3}(w_{s,xy}-w_{b,xy})-\frac{8z^2w_{s,xy}}{3h^2}\,,$$

$$\eta_{zxz}^{(1)}=\eta_{xzz}^{(1)}=\eta_{zzx}^{(1)}=\frac{z}{5}(w_{b,xxx}+w_{b,xyy})+\frac{4z^3}{15h^2}(w_{s,xxx}+w_{s,xyy})-\frac{32zw_{s,x}}{15h^2}\,,$$

$$\eta_{yyy}^{(1)}=\frac{z}{5}(3w_{b,xxy}-2w_{b,yyy})+\frac{4z^3}{15h^2}(3w_{s,xxy}-2w_{s,yyy})+\frac{8zw_{s,y}}{5h^2}\,,$$

$$\eta_{zyy}^{(1)}=\eta_{yyz}^{(1)}=\eta_{yzy}^{(1)}=\frac{1}{15}(w_{b,xx}-w_{s,xx}-4w_{b,yy}+4w_{s,yy})-\frac{8z^2}{15h^2}(4w_{s,yy}-w_{s,xx})\,,$$

$$\eta_{yzz}^{(1)}=\eta_{yzz}^{(1)}=\eta_{zzy}^{(1)}=\frac{z}{5}(w_{b,xxy}+w_{b,yyy})-\frac{32zw_{s,y}}{15h^2}+\frac{4z^3}{15h^2}(w_{s,xxy}+w_{s,yyy})\,,$$

$$\eta_{zzz}^{(1)}=\frac{1}{5}(w_{b,xx}+w_{b,yy}-w_{s,xx}-w_{s,yy})+\frac{8z^2}{5h^2}(w_{s,xx}+w_{s,yy}) \tag{7}$$

$$\chi_{xx}^{(s)}=\left(\frac{1}{2}+\frac{2z^2}{h^2}\right)w_{s,xy}+w_{b,xy}\,,$$

$$\chi_{xy}^{(s)}=\frac{1}{2}(2w_{b,yy}-2w_{b,xx}+w_{s,yy}-w_{s,xx})+\frac{z^2}{h^2}(w_{s,yy}-w_{s,xx})\,,$$

$$\chi_{xz}^{(s)}=\frac{2zw_{s,y}}{h^2}\,,\chi_{yy}^{(s)}=-\left(\frac{1}{2}+\frac{2z^2}{h^2}\right)w_{s,xy}-w_{b,xy}\,,$$

$$\chi_{yz}^{(s)}=-2\frac{zw_{s,x}}{h^2} \tag{8}$$

考虑式(1)、式(3)以及式(5)~式(8),可得微板的变形能

$$\begin{aligned}\Pi_s=\int_\Omega[&\Sigma_1w_{b,xxx}^2+\Sigma_1w_{b,yyy}^2+\Sigma_2w_{b,xxy}^2+\Sigma_2w_{b,xyy}^2+\\&\Sigma_3w_{s,xxx}^2+\Sigma_3w_{s,yyy}^2+\Sigma_4w_{s,xxy}^2+\Sigma_4w_{s,xyy}^2+\\&\Sigma_5w_{b,xxx}w_{s,xxx}+\Sigma_5w_{b,yyy}w_{s,yyy}+\Sigma_6w_{b,xxy}w_{s,yyy}+\\&\Sigma_6w_{b,xxx}w_{s,xyy}+\Sigma_6w_{s,xxy}w_{b,yyy}+\Sigma_6w_{s,xxx}w_{b,xyy}+\\&\Sigma_7w_{b,xxy}w_{b,yyy}+\Sigma_7w_{b,xxx}w_{b,xyy}+\Sigma_8w_{b,xxy}w_{s,xxy}+\\&\Sigma_8w_{b,xyy}w_{s,xyy}+\Sigma_9w_{s,xxy}w_{s,yyy}+\Sigma_9w_{s,xxx}w_{s,xyy}+\\&\frac{\Sigma_{10}}{5}(w_{s,xxx}+w_{s,xyy})w_{s,x}+\frac{\Sigma_{10}}{5}(w_{s,xxy}+w_{s,yyy})w_{s,y}+\\&\Sigma_{10}(w_{b,xxy}+w_{b,yyy})w_{s,y}+\Sigma_{10}(w_{b,xxx}+\\&w_{b,xyy})w_{s,x}+\Sigma_{11}w_{b,xy}^2+\Sigma_{12}w_{s,xy}^2+\Sigma_{13}w_{b,xx}^2+\\&\Sigma_{13}w_{b,yy}^2+\Sigma_{14}w_{s,xx}^2+\Sigma_{14}w_{s,yy}^2+\Sigma_{15}w_{b,xx}w_{s,yy}+\\&\Sigma_{15}w_{s,xx}w_{b,yy}+\Sigma_{16}w_{s,xx}w_{b,xx}+\Sigma_{16}w_{s,yy}w_{b,yy}+\\&\Sigma_{18}w_{b,xx}w_{b,yy}+\Sigma_{17}w_{s,xx}w_{s,yy}+\Sigma_{19}w_{s,xy}w_{b,xy}+\\&\Sigma_{20}w_{s,y}^2+\Sigma_{20}w_{s,x}^2]\,\mathrm{d}\Omega\end{aligned} \tag{9}$$

式中,Σ_i 为刚度系数,具体表达式参见附录 A。

基于式(4)可得微板的动能

$$\Pi_d=\int_\Omega\left[\frac{\rho h}{2}(w_{b,t}^2+2w_{b,t}w_{s,t}+w_{s,t}^2)+\frac{\rho h^3}{24}(w_{b,xt}^2+w_{b,yt}^2)+\frac{\rho h^3}{60}(w_{b,xt}w_{s,xt}+w_{b,yt}w_{s,yt})+\frac{\rho h^3}{504}(w_{s,xt}^2+w_{s,yt}^2)\right]\mathrm{d}\Omega \tag{10}$$

考虑式(9)和式(10),可得微板自由振动的 Euler-Lagrange 方程

$$2\Sigma_1(w_{b,xxxxxx}+w_{b,yyyyyy})+2(\Sigma_2+\Sigma_7)(w_{b,xxxxyy}+w_{b,xxyyyy})+\Sigma_5(w_{s,xxxxxx}+w_{s,yyyyyy})+(2\Sigma_6+\Sigma_8)(w_{s,xxxxyy}+w_{s,xxyyyy})+(\Sigma_{10}-\Sigma_{16})(w_{s,xxxx}+w_{s,yyyy})-2\Sigma_{13}(w_{b,xxxx}+w_{b,yyyy})+(2\Sigma_{10}-2\Sigma_{15}-\Sigma_{19})w_{s,xxyy}-2(\Sigma_{11}+\Sigma_{18})w_{b,xxyy}-\rho h(w_{s,tt}+w_{b,tt})+\frac{\rho h^3}{60}(w_{s,yytt}+w_{s,xxtt})+\frac{\rho h^3}{12}(w_{b,yytt}+w_{b,xxtt})=0 \tag{11}$$

$$2(\Sigma_4+\Sigma_9)(w_{s,xxxxyy}+w_{s,xxyyyy})+\Sigma_5(w_{b,xxxxxx}+w_{b,yyyyyy})+(\Sigma_8+2\Sigma_6)(w_{b,xxxxyy}+w_{b,xxyyyy})+2\Sigma_3(w_{s,xxxxxx}+w_{s,yyyyyy})+2\left(\frac{\Sigma_{10}}{5}-\Sigma_{14}\right)(w_{s,xxxx}+w_{s,yyyy})+(2\Sigma_{10}-2\Sigma_{15}-\Sigma_{19})w_{b,xxyy}+2\left(\frac{2\Sigma_{10}}{5}-\Sigma_{12}-\Sigma_{17}\right)w_{s,xxyy}+(\Sigma_{10}-\Sigma_{16})(w_{b,xxxx}+w_{b,yyyy})+2\Sigma_{20}(w_{s,xx}+w_{s,yy})-\rho h(w_{s,tt}+w_{b,tt})+\frac{\rho h^3}{60}(w_{b,yytt}+w_{b,xxtt})+\frac{\rho h^3}{252}(w_{s,yytt}+w_{s,xxtt})=0 \tag{12}$$

对于四边简支微板,其挠度分量 w_b 和 w_s 可以表示为 Navier 级数形式

$$w_b = \sum_{m=1}^{\infty}\sum_{n=1}^{\infty} W_b \sin(\alpha_m x)\sin(\beta_n y)\mathrm{e}^{j\omega t},$$
$$w_s = \sum_{m=1}^{\infty}\sum_{n=1}^{\infty} W_s \sin(\alpha_m x)\sin(\beta_n y)\mathrm{e}^{j\omega t} \tag{13}$$

式中:$\alpha_m = m\pi/L_x$;$\beta_n = n\pi/L_y$;m、n 分别为 x、y 方向半波数;W_b 和 W_s 分别为纯弯曲和纯剪切变形引起的挠度幅值。

将式(13)代入式(11)和式(12)可得

$$\left(\begin{bmatrix} K_{11}^{(mn)} & K_{12}^{(mn)} \\ K_{21}^{(mn)} & K_{22}^{(mn)} \end{bmatrix} - \omega^2 \begin{bmatrix} M_{11}^{(mn)} & M_{12}^{(mn)} \\ M_{21}^{(mn)} & M_{22}^{(mn)} \end{bmatrix}\right)\begin{bmatrix} W_b \\ W_s \end{bmatrix} = \begin{bmatrix} 0 \\ 0 \end{bmatrix} \tag{14}$$

式中:

$$\begin{aligned} K_{11}^{(mn)} &= 2\Sigma_1(\alpha_m^6+\beta_n^6) + 2(\Sigma_2+\Sigma_7)\alpha_m^2\beta_n^2(\alpha_m^2+\beta_n^2) + \\ &\quad 2\Sigma_{13}(\alpha_m^4+\beta_n^4) + 2(\Sigma_{11}+\Sigma_{18})\alpha_m^2\beta_n^2, \\ K_{21}^{(mn)} &= K_{12}^{(mn)} \\ &= \Sigma_5(\alpha_m^6+\beta_n^6) + (2\Sigma_6+\Sigma_8)\alpha_m^2\beta_n^2(\alpha_m^2+\beta_n^2) + \\ &\quad (\Sigma_{16}-\Sigma_{10})(\alpha_m^4+\beta_n^4) + \\ &\quad (2\Sigma_{15}+\Sigma_{19}-2\Sigma_{10})\alpha_m^2\beta_n^2, \\ K_{22}^{(mn)} &= 2\Sigma_3(\alpha_m^6+\beta_n^6) + 2\left(\Sigma_{14}-\frac{\Sigma_{10}}{5}\right)(\alpha_m^4+\beta_n^4) + \\ &\quad 2(\Sigma_4+\Sigma_9)\alpha_m^2\beta_n^2(\alpha_m^2+\beta_n^2) + 2\Sigma_{20}(\alpha_m^2+\beta_n^2) + \\ &\quad 2\left(\Sigma_{17}+\Sigma_{12}-\frac{2\Sigma_{10}}{5}\right)\alpha_m^2\beta_n^2 \end{aligned} \tag{15}$$

$$M_{11}^{(mn)} = \frac{\rho h^3(\alpha_m^2+\beta_n^2)}{12} + \rho h,$$
$$M_{21}^{(mn)} = M_{12}^{(mn)} = \frac{\rho h^3(\alpha_m^2+\beta_n^2)}{60} + \rho h,$$
$$M_{22}^{(mn)} = \frac{\rho h^3(\alpha_m^2+\beta_n^2)}{252} + \rho h \tag{16}$$

2　微分求积有限元

从式(9)、式(11)和式(12)可以看出,本研究模型受控于 2 个六阶偏微分方程,且要求 w_b 和 w_s 满足 C^2 连续性,因而解析求解将变得十分困难。近些年来,邹星等[27-32]融合 Gauss-Lobatto 求积准则和微分求积准则构造了应变梯度 Euler-Bernoulli 梁、Timoshenko 梁、Reddy 梁、Kirchhoff 板、Mindlin 板、精化高阶剪切变形梁以及修正的偶应力精化高阶剪切变形板[13-14]的微分求积有限元法。本研究将该方法进一步拓展至应变梯度高阶剪切变形板的情形。鉴于本研究模型 w_b 和 w_s 的 C^2 连续性要求,图 2 给出单元域 $[0,2a]\times[0,2b]$ 上的微分求积几何映射策略以及 Gauss-Lobatto(简写为 GL)求积点坐标。

单元域上 w_b 的 Lagrange 插值形式为

$$w_b = \sum_{i=1}^{6}\sum_{j=1}^{6} l_i(x)l_j(y)\langle w_b\rangle_{(x_i,y_j)} \tag{17}$$

式中:$\langle w_b\rangle_{(x_i,y_j)}$ 为单元 GL 求积点 (x_i,y_j) 的挠度;$l_i(x)$、$l_j(y)$ 分别为 x 方向第 i 个、y 方向第 j 个插值基函数。根据微分求积准则可将 w_b 在单元 GL 求积点处各阶导数表示为矩阵形式,即

$$\left[\frac{\partial^{m+n}w_b}{\partial x^m\partial y^n}\right]_{\mathrm{GL}} = \boldsymbol{D}_x^{(m)}\boldsymbol{D}_y^{(m)}[w_b]_{\mathrm{GL}},$$
$$\left[\frac{\partial^m w_b}{\partial x^m}\right]_{\mathrm{GL}} = \boldsymbol{D}_x^{(m)}[w_b]_{\mathrm{GL}},\quad \left[\frac{\partial^n w_b}{\partial y^n}\right]_{\mathrm{GL}} = \boldsymbol{D}_y^{(n)}[w_b]_{\mathrm{GL}} \tag{18}$$

式中:

$$\begin{aligned} \left[\frac{\partial^{m+n}w_b}{\partial x^m\partial y^n}\right]_{\mathrm{GL}} = \Bigg[&\left\langle\frac{\partial^{m+n}w_b}{\partial x^m\partial y^n}\right\rangle_{(x_1,y_1)} \left\langle\frac{\partial^{m+n}w_b}{\partial x^m\partial y^n}\right\rangle_{(x_2,y_1)} \cdots \left\langle\frac{\partial^{m+n}w_b}{\partial x^m\partial y^n}\right\rangle_{(x_6,y_1)} \\ &\left\langle\frac{\partial^{m+n}w_b}{\partial x^m\partial y^n}\right\rangle_{(x_1,y_2)} \left\langle\frac{\partial^{m+n}w_b}{\partial x^m\partial y^n}\right\rangle_{(x_2,y_2)} \cdots \left\langle\frac{\partial^{m+n}w_b}{\partial x^m\partial y^n}\right\rangle_{(x_6,y_2)} \\ &\vdots \\ &\left\langle\frac{\partial^{m+n}w_b}{\partial x^m\partial y^n}\right\rangle_{(x_1,y_6)} \left\langle\frac{\partial^{m+n}w_b}{\partial x^m\partial y^n}\right\rangle_{(x_2,y_6)} \cdots \left\langle\frac{\partial^{m+n}w_b}{\partial x^m\partial y^n}\right\rangle_{(x_6,y_6)} \Bigg]^{\mathrm{T}}, \end{aligned}$$

$$[w_b]_{\mathrm{GL}} = \left\langle\left[\frac{\partial^{m+n}w_b}{\partial x^m\partial y^n}\right]_{\mathrm{GL}}\right\rangle_{m=n=0},\quad \left[\frac{\partial^m w_b}{\partial x^m}\right]_{\mathrm{GL}} = \left\langle\left[\frac{\partial^{m+n}w_b}{\partial x^m\partial y^n}\right]_{\mathrm{GL}}\right\rangle_{n=0},\quad \left[\frac{\partial^n w_b}{\partial y^n}\right]_{\mathrm{GL}} = \left\langle\left[\frac{\partial^{m+n}w_b}{\partial x^m\partial y^n}\right]_{\mathrm{GL}}\right\rangle_{m=0} \tag{19}$$

微分求积系数矩阵 $\boldsymbol{D}_x^{(m)}$ 和 $\boldsymbol{D}_y^{(n)}$ 的具体形式可参见文献[30]中式(37)~式(39)。若采用式(18)离散微板单元的变形能和动能,所得表达式仅包含单元 GL 求积点处挠度本身。为满足单元间协调性要求,需要将单元 GL 求积点处位移参数转换为单元节点处位移参数。引入单元节点位移向量 $[w_b]_{\mathrm{N}}$。

$$[w_b]_{\mathrm{N}} = [\langle w_b\rangle_{(x_1,y_1)} \quad \langle w_{b,x}\rangle_{(x_1,y_1)} \quad \langle w_{b,y}\rangle_{(x_1,y_1)} \quad \langle w_{b,xx}\rangle_{(x_1,y_1)} \quad \langle w_{b,yy}\rangle_{(x_1,y_1)} \quad \langle w_{b,xy}\rangle_{(x_1,y_1)}$$
$$\langle w_{b,xxy}\rangle_{(x_1,y_1)} \quad \langle w_{b,xyy}\rangle_{(x_1,y_1)} \quad \langle w_{b,xxyy}\rangle_{(x_1,y_1)} \quad \langle w_b\rangle_{(x_6,y_1)} \quad \cdots \quad \langle w_{b,xxyy}\rangle_{(x_6,y_1)}$$
$$\langle w_b\rangle_{(x_6,y_6)} \quad \cdots \quad \langle w_{b,xxyy}\rangle_{(x_6,y_6)} \quad \langle w_b\rangle_{(x_1,y_6)} \quad \cdots \quad \langle w_{b,xxyy}\rangle_{(x_1,y_6)}]^{\mathrm{T}} \tag{20}$$

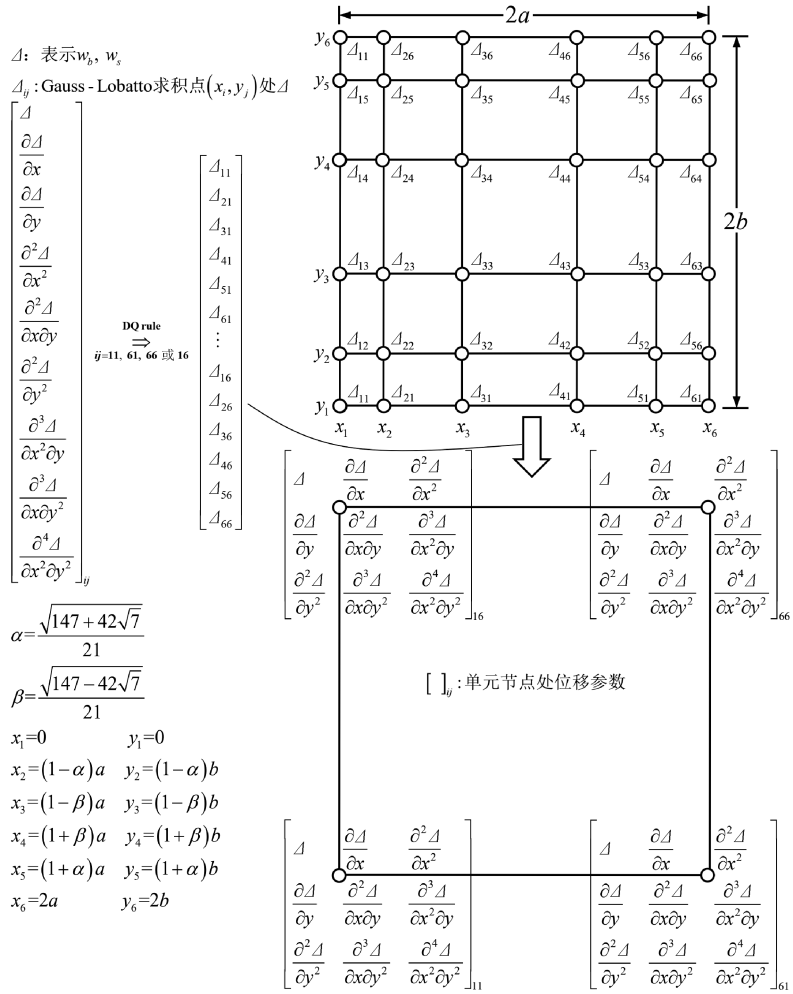

图 2 微板单元的微分求积几何映射策略

Fig. 2 Differential quadrature-based geometric mapping scheme for thepresent microplate element

利用微分求积准则可得

$$[w_b]_{\mathrm{N}} = \boldsymbol{B}[w_b]_{\mathrm{GL}} \tag{21}$$

式中：$\boldsymbol{B}$ 为转换矩阵，其表达式见文献[30]中式(45)。

利用式(18)和式(21)可将式(9)离散为

$$\Pi_s = ([w_b]_{\mathrm{N}})^{\mathrm{T}}(\boldsymbol{B}^{-1})^{\mathrm{T}}\boldsymbol{K}_{(w_bw_b)}\boldsymbol{B}^{-1}[w_b]_{\mathrm{N}} + ([w_s]_{\mathrm{N}})^{\mathrm{T}}(\boldsymbol{B}^{-1})^{\mathrm{T}}\boldsymbol{K}_{(w_sw_s)}\boldsymbol{B}^{-1}[w_s]_{\mathrm{N}} + ([w_b]_{\mathrm{N}})^{\mathrm{T}}(\boldsymbol{B}^{-1})^{\mathrm{T}}\boldsymbol{K}_{(w_bw_s)}\boldsymbol{B}^{-1}[w_s]_{\mathrm{N}} \tag{22}$$

$$\boldsymbol{K}_{(w_bw_b)} = \Sigma_1(\boldsymbol{D}_x^{(3)})^{\mathrm{T}}\boldsymbol{Q}_{\mathrm{GL}}\boldsymbol{D}_x^{(3)} + \Sigma_1(\boldsymbol{D}_y^{(3)})^{\mathrm{T}}\boldsymbol{Q}_{\mathrm{GL}}\boldsymbol{D}_y^{(3)} + \Sigma_2(\boldsymbol{D}_{xy}^{(2\oplus1)})^{\mathrm{T}}\boldsymbol{Q}_{\mathrm{GL}}\boldsymbol{D}_{xy}^{(2\oplus1)} + \Sigma_2(\boldsymbol{D}_{xy}^{(1\oplus2)})^{\mathrm{T}}\boldsymbol{Q}_{\mathrm{GL}}\boldsymbol{D}_{xy}^{(1\oplus2)} + \Sigma_7(\boldsymbol{D}_{xy}^{(2\oplus1)})^{\mathrm{T}}\boldsymbol{Q}_{\mathrm{GL}}\boldsymbol{D}_y^{(3)} + \Sigma_7(\boldsymbol{D}_x^{(3)})^{\mathrm{T}}\boldsymbol{Q}_{\mathrm{GL}}\boldsymbol{D}_y^{(1\oplus2)} + \Sigma_{11}(\boldsymbol{D}_{xy}^{(1\oplus1)})^{\mathrm{T}}\boldsymbol{Q}_{\mathrm{GL}}\boldsymbol{D}_{xy}^{(1\oplus1)} + \Sigma_{13}(\boldsymbol{D}_y^{(2)})^{\mathrm{T}}\boldsymbol{Q}_{\mathrm{GL}}\boldsymbol{D}_y^{(2)} + \Sigma_{18}(\boldsymbol{D}_x^{(2)})^{\mathrm{T}}\boldsymbol{Q}_{\mathrm{GL}}\boldsymbol{D}_y^{(2)} + \Sigma_{13}(\boldsymbol{D}_x^{(2)})^{\mathrm{T}}\boldsymbol{Q}_{\mathrm{GL}}\boldsymbol{D}_x^{(2)} \tag{23a}$$

$$\boldsymbol{K}_{(w_sw_s)} = \Sigma_3(\boldsymbol{D}_x^{(3)})^{\mathrm{T}}\boldsymbol{Q}_{\mathrm{GL}}\boldsymbol{D}_x^{(3)} + \Sigma_3(\boldsymbol{D}_y^{(3)})^{\mathrm{T}}\boldsymbol{Q}_{\mathrm{GL}}\boldsymbol{D}_y^{(3)} + \Sigma_4(\boldsymbol{D}_{xy}^{(2\oplus1)})^{\mathrm{T}}\boldsymbol{Q}_{\mathrm{GL}}\boldsymbol{D}_{xy}^{(2\oplus1)} + \Sigma_4(\boldsymbol{D}_{xy}^{(1\oplus2)})^{\mathrm{T}}\boldsymbol{Q}_{\mathrm{GL}}\boldsymbol{D}_{xy}^{(1\oplus2)} + \Sigma_9(\boldsymbol{D}_{xy}^{(2\oplus1)})^{\mathrm{T}}\boldsymbol{Q}_{\mathrm{GL}}\boldsymbol{D}_y^{(3)} + \Sigma_9(\boldsymbol{D}_x^{(3)})^{\mathrm{T}}\boldsymbol{Q}_{\mathrm{GL}}\boldsymbol{D}_y^{(1\oplus2)} + \frac{\Sigma_{10}}{5}(\boldsymbol{D}_x^{(3)})^{\mathrm{T}}\boldsymbol{Q}_{\mathrm{GL}}\boldsymbol{D}_x^{(1)} + \frac{\Sigma_{10}}{5}(\boldsymbol{D}_{xy}^{(1\oplus2)})^{\mathrm{T}}\boldsymbol{Q}_{\mathrm{GL}}\boldsymbol{D}_x^{(1)} + \frac{\Sigma_{10}}{5}(\boldsymbol{D}_y^{(3)})^{\mathrm{T}}\boldsymbol{Q}_{\mathrm{GL}}\boldsymbol{D}_y^{(1)} + \frac{\Sigma_{10}}{5}(\boldsymbol{D}_{xy}^{(2\oplus1)})^{\mathrm{T}}\boldsymbol{Q}_{\mathrm{GL}}\boldsymbol{D}_y^{(1)} + \Sigma_{12}(\boldsymbol{D}_{xy}^{(1\oplus1)})^{\mathrm{T}}\boldsymbol{Q}_{\mathrm{GL}}\boldsymbol{D}_{xy}^{(1\oplus1)} + \Sigma_{14}(\boldsymbol{D}_x^{(2)})^{\mathrm{T}}\boldsymbol{Q}_{\mathrm{GL}}\boldsymbol{D}_x^{(2)} +$$

$$\Sigma_{14}\left(\boldsymbol{D}_y^{(2)}\right)^{\mathrm{T}}\boldsymbol{Q}_{\mathrm{GL}}\boldsymbol{D}_y^{(2)}+\Sigma_{17}\left(\boldsymbol{D}_x^{(2)}\right)^{\mathrm{T}}\boldsymbol{Q}_{\mathrm{GL}}\boldsymbol{D}_y^{(2)}+\Sigma_{20}\left(\boldsymbol{D}_y^{(1)}\right)^{\mathrm{T}}\boldsymbol{Q}_{\mathrm{GL}}\boldsymbol{D}_y^{(1)}+\Sigma_{20}\left(\boldsymbol{D}_x^{(1)}\right)^{\mathrm{T}}\boldsymbol{Q}_{\mathrm{GL}}\boldsymbol{D}_x^{(1)} \tag{23b}$$

$$\begin{aligned}\boldsymbol{K}_{(w_b w_s)}=&\Sigma_5\left(\boldsymbol{D}_x^{(3)}\right)^{\mathrm{T}}\boldsymbol{Q}_{\mathrm{GL}}\boldsymbol{D}_x^{(3)}+\Sigma_5\left(\boldsymbol{D}_y^{(3)}\right)^{\mathrm{T}}\boldsymbol{Q}_{\mathrm{GL}}\boldsymbol{D}_y^{(3)}+\Sigma_6\left(\boldsymbol{D}_{xy}^{(2\oplus1)}\right)^{\mathrm{T}}\boldsymbol{Q}_{\mathrm{GL}}\boldsymbol{D}_y^{(3)}+\Sigma_6\left(\boldsymbol{D}_x^{(3)}\right)^{\mathrm{T}}\boldsymbol{Q}_{\mathrm{GL}}\boldsymbol{D}_y^{(1\oplus2)}+\\&\Sigma_6\left(\boldsymbol{D}_{xy}^{(2\oplus1)}\right)^{\mathrm{T}}\boldsymbol{Q}_{\mathrm{GL}}\boldsymbol{D}_y^{(3)}+\Sigma_6\left(\boldsymbol{D}_{xy}^{(1\oplus2)}\right)^{\mathrm{T}}\boldsymbol{Q}_{\mathrm{GL}}\boldsymbol{D}_x^{(3)}+\Sigma_8\left(\boldsymbol{D}_{xy}^{(2\oplus1)}\right)^{\mathrm{T}}\boldsymbol{Q}_{\mathrm{GL}}\boldsymbol{D}_{xy}^{(2\oplus1)}+\Sigma_8\left(\boldsymbol{D}_{xy}^{(2\oplus1)}\right)^{\mathrm{T}}\boldsymbol{Q}_{\mathrm{GL}}\boldsymbol{D}_{xy}^{(2\oplus1)}+\\&\Sigma_{10}\left(\boldsymbol{D}_{xy}^{(2\oplus1)}\right)^{\mathrm{T}}\boldsymbol{Q}_{\mathrm{GL}}\boldsymbol{D}_y^{(1)}+\Sigma_{10}\left(\boldsymbol{D}_y^{(3)}\right)^{\mathrm{T}}\boldsymbol{Q}_{\mathrm{GL}}\boldsymbol{D}_y^{(1)}+\Sigma_{10}\left(\boldsymbol{D}_x^{(3)}\right)^{\mathrm{T}}\boldsymbol{Q}_{\mathrm{GL}}\boldsymbol{D}_x^{(1)}+\Sigma_{10}\left(\boldsymbol{D}_{xy}^{(1\oplus2)}\right)^{\mathrm{T}}\boldsymbol{Q}_{\mathrm{GL}}\boldsymbol{D}_x^{(1)}+\\&\Sigma_{15}\left(\boldsymbol{D}_x^{(2)}\right)^{\mathrm{T}}\boldsymbol{Q}_{\mathrm{GL}}\boldsymbol{D}_y^{(2)}+\Sigma_{15}\left(\boldsymbol{D}_y^{(2)}\right)^{\mathrm{T}}\boldsymbol{Q}_{\mathrm{GL}}\boldsymbol{D}_x^{(2)}+\Sigma_{16}\left(\boldsymbol{D}_x^{(2)}\right)^{\mathrm{T}}\boldsymbol{Q}_{\mathrm{GL}}\boldsymbol{D}_x^{(2)}+\Sigma_{16}\left(\boldsymbol{D}_y^{(2)}\right)^{\mathrm{T}}\boldsymbol{Q}_{\mathrm{GL}}\boldsymbol{D}_y^{(2)}+\\&\Sigma_{19}\left(\boldsymbol{D}_{xy}^{(1\oplus1)}\right)^{\mathrm{T}}\boldsymbol{Q}_{\mathrm{GL}}\boldsymbol{D}_{xy}^{(1\oplus1)}\end{aligned} \tag{23c}$$

式中:$\boldsymbol{D}_{xy}^{(m\oplus n)}$ 表示位移变量对 x 的 m 阶偏导数和对 y 的 n 阶偏导数对应于的微分求积系数矩阵;$\boldsymbol{Q}_{\mathrm{GL}}$ 为单元 GL 求积点处权系数矩阵,具体形式参见文献[30]中式(42)。

利用式(18)和式(21)可将式(10)离散为

$$\begin{aligned}\Pi_d=&\left([\dot{w}_b]_{\mathrm{N}}\right)^{\mathrm{T}}\left(\boldsymbol{B}^{-1}\right)^{\mathrm{T}}\left[\frac{\rho h}{2}Q_{\mathrm{GL}}+\frac{\rho h^3}{24}\left(D_x^{(1)}\right)^{\mathrm{T}}Q_{\mathrm{GL}}D_x^{(1)}+\frac{\rho h^3}{24}\left(D_y^{(1)}\right)^{\mathrm{T}}Q_{\mathrm{GL}}D_y^{(1)}\right]\boldsymbol{B}^{-1}[\dot{w}_b]_{\mathrm{N}}+\\&\left([\dot{w}_s]_{\mathrm{N}}\right)^{\mathrm{T}}\left(\boldsymbol{B}^{-1}\right)^{\mathrm{T}}\left[\frac{\rho h}{2}Q_{\mathrm{GL}}+\frac{\rho h^3}{504}\left(D_x^{(1)}\right)^{\mathrm{T}}Q_{\mathrm{GL}}D_x^{(1)}+\frac{\rho h^3}{504}\left(D_y^{(1)}\right)^{\mathrm{T}}Q_{\mathrm{GL}}D_y^{(1)}\right]\boldsymbol{B}^{-1}[\dot{w}_s]_{\mathrm{N}}+\\&\left([\dot{w}_b]_{\mathrm{N}}\right)^{\mathrm{T}}\left(\boldsymbol{B}^{-1}\right)^{\mathrm{T}}\left[\rho hQ_{\mathrm{GL}}+\frac{\rho h^3}{60}\left(D_x^{(1)}\right)^{\mathrm{T}}Q_{\mathrm{GL}}D_x^{(1)}+\frac{\rho h^3}{60}\left(D_y^{(1)}\right)^{\mathrm{T}}Q_{\mathrm{GL}}D_y^{(1)}\right]\boldsymbol{B}^{-1}[\dot{w}_s]_{\mathrm{N}}\end{aligned} \tag{24}$$

为推导单元刚度矩阵 $\boldsymbol{K}^{(e)}$ 和质量矩阵 $\boldsymbol{M}^{(e)}$,引入单元节点总体位移向量

$$\begin{aligned}\Delta_{\mathrm{N}}=[&\langle w_b\rangle_{(x_1,y_1)}\ \langle w_s\rangle_{(x_1,y_1)}\ \langle w_{b,x}\rangle_{(x_1,y_1)}\ \langle w_{s,x}\rangle_{(x_1,y_1)}\ \cdots\ \langle w_{b,xxyy}\rangle_{(x_1,y_1)}\ \langle w_{s,xxyy}\rangle_{(x_1,y_1)}\\&\langle w_b\rangle_{(x_6,y_1)}\ \langle w_s\rangle_{(x_6,y_1)}\ \langle w_{b,x}\rangle_{(x_6,y_1)}\ \langle w_{s,x}\rangle_{(x_6,y_1)}\ \cdots\ \langle w_{b,xxyy}\rangle_{(x_6,y_1)}\ \langle w_{s,xxyy}\rangle_{(x_6,y_1)}\\&\langle w_b\rangle_{(x_6,y_6)}\ \langle w_s\rangle_{(x_6,y_6)}\ \langle w_{b,x}\rangle_{(x_6,y_6)}\ \langle w_{s,x}\rangle_{(x_6,y_6)}\ \cdots\ \langle w_{b,xxyy}\rangle_{(x_6,y_6)}\ \langle w_{s,xxyy}\rangle_{(x_6,y_6)}\\&\langle w_b\rangle_{(x_1,y_6)}\ \langle w_s\rangle_{(x_1,y_6)}\ \langle w_{b,x}\rangle_{(x_1,y_6)}\ \langle w_{s,x}\rangle_{(x_1,y_6)}\ \cdots\ \langle w_{b,xxyy}\rangle_{(x_1,y_6)}\ \langle w_{s,xxyy}\rangle_{(x_1,y_6)}]^{\mathrm{T}}\end{aligned} \tag{25}$$

于是 $\boldsymbol{K}^{(e)}$ 和 $\boldsymbol{M}^{(e)}$ 的具体元素可以表示为

$$\boldsymbol{K}_{ij}^{(e)}=\frac{\partial^2\Pi_s}{\partial\Delta_{\mathrm{N}}(i)\partial\Delta_{\mathrm{N}}(j)},\ \boldsymbol{M}_{ij}^{(e)}=\frac{\partial^2\Pi_d}{\partial\dot{\Delta}_{\mathrm{N}}(i)\partial\dot{\Delta}_{\mathrm{N}}(j)} \tag{26}$$

其解析表达式可采用 MAPLE 符号计算软件导出。

矩形微板常见约束有固支(C)、简支(S)和自由(F),数值实施中具体设置如下。

固支(C)约束

$$w_b=w_s=\frac{\partial w_b}{\partial x}=\frac{\partial w_s}{\partial x}=\frac{\partial w_b}{\partial y}=\frac{\partial w_s}{\partial y}\Big|_{x=0\ \text{or}\ x=L_x}=0 \tag{27a}$$

$$w_b=w_s=\frac{\partial w_b}{\partial x}=\frac{\partial w_s}{\partial x}=\frac{\partial w_b}{\partial y}=\frac{\partial w_s}{\partial y}\Big|_{y=0\ \text{or}\ y=L_y}=0 \tag{27b}$$

简支(S)约束

$$w_b=w_s=\frac{\partial w_b}{\partial y}=\frac{\partial w_s}{\partial y}\Big|_{x=0\ \text{or}\ x=L_x}=0 \tag{28a}$$

$$w_b=w_s=\frac{\partial w_b}{\partial x}=\frac{\partial w_s}{\partial x}\Big|_{y=0\ \text{or}\ y=L_y}=0 \tag{28b}$$

自由(F):无位移约束。

图 3 给出了不同边界条件下微板的示意图,边线依照左边-下边-右边-上边排序。

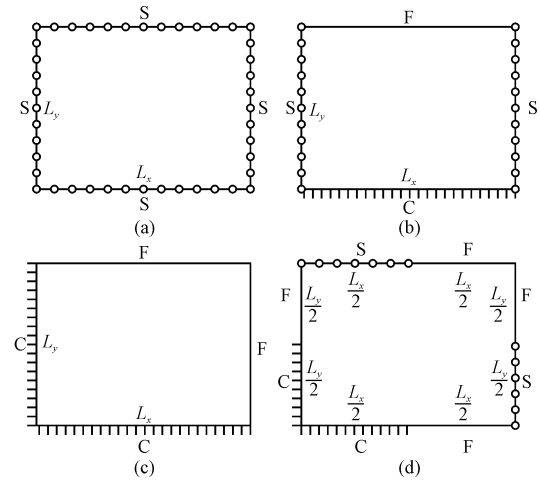

图 3　4 种边界条件下微板的示意图

Fig. 3　Schematic of a microplate under four types of boundary conditions

3　数值结果与讨论

本节通过若干数值算例,验证本研究微分求积有限元的有效性,探究微板无量纲频率及模态振型随长宽比、长厚比、材料尺度参数、边界条件的变化规律。假定微板由环氧树脂组成,弹性模量 E =

1.44 GPa，泊松比 $\nu = 0.3$，密度 $\rho = 1\,220\ \mathrm{kg/m^3}$。需要指出的是，MSGT 中 3 个材料尺度参数并无内在数值关联。为简单起见，本研究取 $l_0 = l_1 = l_2 = l = 15\ \mu\mathrm{m}$。引入以下无量纲参数。

$$\varpi_n = \frac{\omega_n L_y^2}{\pi^2}\sqrt{\frac{\rho h}{D}} \tag{29}$$

3.1 有效性验证

文献[30]对应变梯度 Kirchhoff 微板的微分求积有限元的收敛性开展了深入研究，发现在相同节点参数配置下微分求积有限元比标准有限元具有更低的单元矩阵条件数。因此，本节仅对微分求积有限元的收敛性做简单讨论。图 4 呈现了 SSSS 和 SCSF 微板前 5 阶无量纲频率随网格数的变化。此处，$L_x/L_y = 1$，$L_x/h = 8$，$l/h = 1$。从图 4 可以看到，随着网格的增多，前 5 阶无量纲频率值均趋于稳定值。除非特别说明，以下计算中网格密度为 30×30。

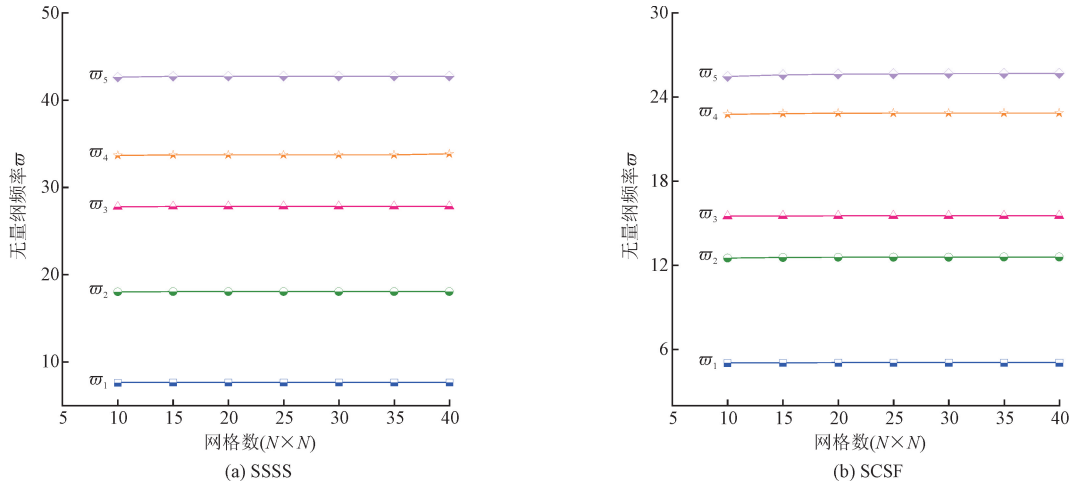

(a) SSSS (b) SCSF

图 4 微板前 5 阶无量纲频率的收敛性

Fig. 4 Convergence of the first five dimensionless frequencies fora microplate

表 1 列出了不考虑尺度效应时（$l/h = 0$）本研究 C^2 型和文献[31]中 C^2 型微分求积有限元所预测的环氧树脂 Kirchhoff 微板的前 5 阶无量纲频率。表 2 列出来考虑尺度效应时（$l/h = 1$）两种单元所预测的前两阶无量纲频率。

同时，两表也给出了 SSSS 微板振动频率的 Navier 解。为了比较起见，计算参数取为 $L_x = L_y = 100\ \mu\mathrm{m}$，$h = 2\ \mu\mathrm{m}$，$\varpi_n = \omega_n L_y^2\sqrt{\rho h/D}$。从表中可以看出，本研究微分求积有限元预测结果略小于文献[31]中结果，且模态阶次越高，两者差异越显著；对于 SSSS 微板，本研究微分求积有限元预测结果略大于 Navier 解析解。原因在于本研究模型考虑了剪切变形效应，使其刚度小于文献[31]中 Kirchhoff 微板模型的刚度。

表 1 当 $l/h = 0$ 时环氧树脂 Kirchhoff 微板的前 5 阶无量纲频率

Tab. 1 The first five dimensionless frequencies of epoxy resin Kirchhoff microplate ($l/h = 0$)

边界条件	方法	无量纲频率				
		ϖ_1	ϖ_2	ϖ_3	ϖ_4	ϖ_5
SSSS	本研究①	19.625 4	48.647 9	48.647 9	77.192 2	95.966 6
	本研究②	19.707 6	49.153 0	49.153 0	78.456 8	97.924 4
	文献[31]	19.739 0	49.348 0	49.348 0	79.400 0	100.170 0
SFSF	本研究②	9.624 1	16.116 4	36.632 5	38.826 3	46.577 3
	文献[31]	9.614 0	16.135 0	37.180 0	39.134 0	47.280 0
SCSC	本研究②	27.773 3	53.655 5	65.960 2	91.175 6	100.733 0
	文献[31]	28.950 0	54.873 0	69.327 0	94.703 0	103.710 0
SCSF	本研究②	12.588 2	32.393 5	41.500 2	62.141 6	70.477 1
	文献[31]	12.687 0	33.067 0	41.714 0	63.260 0	73.870 0
SCSS	本研究②	23.206 7	51.139 2	57.121 7	84.407 6	99.206 7
	文献[31]	23.646 0	51.813 0	58.650 0	86.252 0	101.800 0

注：①Navier 法；②微分求积有限元法。

表 2　当 $l/h = 1$ 时环氧树脂 Kirchhoff 微板的前 2 阶无量纲频率

Tab. 2　The first two dimensionless frequencies of epoxy resin Kirchhoff microplate ($l/h = 1$)

边界条件	方法	无量纲频率	
		ϖ_1	ϖ_2
SSSS	本研究①	22.897 5	56.228 7
	本研究②	22.993 4	56.812 5
	文献[31]	23.685 6	59.312 4
CFFF	本研究②	4.062 9	10.158 1
	文献[31]	4.165 9	10.269 7
SCSF	本研究②	14.981 6	38.468 6
	文献[31]	15.285 5	39.816 9

3.2　参数分析

图 5 呈现了 SSSS 和 SCSF 微板前 6 阶无量纲频率随无量纲材料尺度参数的变化。从图 5 可以看出,各阶无量纲频率随无量纲材料尺度参数的增大而增大,并且具有“越小越强”的特点,这是由于应变梯度的出现导致了微板刚度增强。图 6 呈现了微板前 6 阶无量纲频比 $\delta = \langle \varpi_n \rangle_{l/h>0} / \langle \varpi_n \rangle_{l/h=0}$ 随无量纲材料尺度参数的变化。从图 6 可以看出,尺度效应对不同阶次模态的影响程度不同:对于 SSSS 微板,模态阶次越高,无量纲频率比越大,这说明尺度效应对 SSSS 微板高阶模态的影响更加显著;对于 SCSF 微板,尺度效应对第 5 阶模态的影响最显著,而对第 1 阶和第 3 阶模态的影响最弱;尺度效应对 SSSS 微板的影响弱于 SCSF 微板。

图 7 给出了 SSSS 微板前 6 阶无量纲频率随长宽比和长厚比的变化。从图 7(a)可以看出,微板各阶无量纲频率随着长宽比增大而减小,但减小趋势会逐渐趋于平缓;模态阶次越高,或无量纲材料尺度参数越大,长宽比对各阶无量纲频率的影响越显著。从图 7(b)可以看出,微板各阶无量纲频率随着长厚比的增大而增大,但增大趋势会逐渐趋于平缓;模态阶次越高或无量纲材料尺度参数越大,长厚比对微板各阶无量纲频率的影响越显著。微板无量纲频率随长宽比和长厚比的变化趋于平缓的原因在于,当长宽比增大时,微板逐渐趋向于细长梁,而当长厚比足够大时,高阶剪切变形效应对微板刚度的影响会变得很微弱。

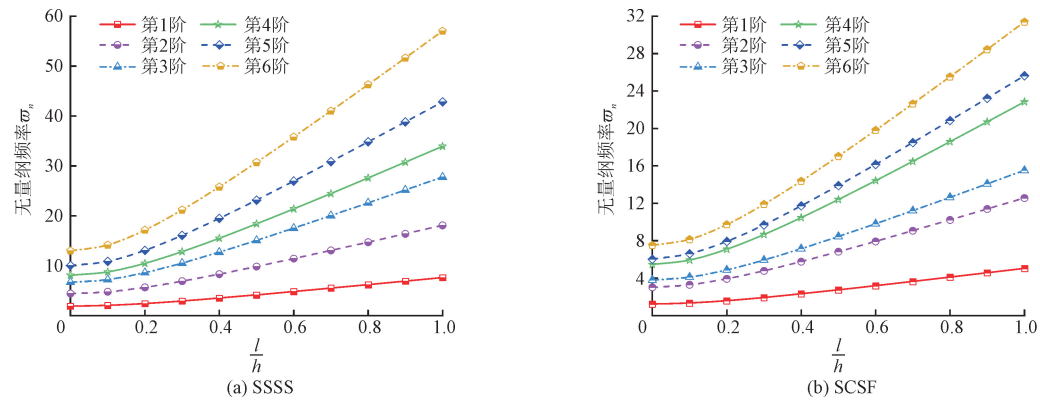

图 5　无量纲材料尺度参数对微板无量纲频率的影响

Fig. 5　Influence of dimensionless material length-scale parameter on the dimensionless frequencies of a microplate

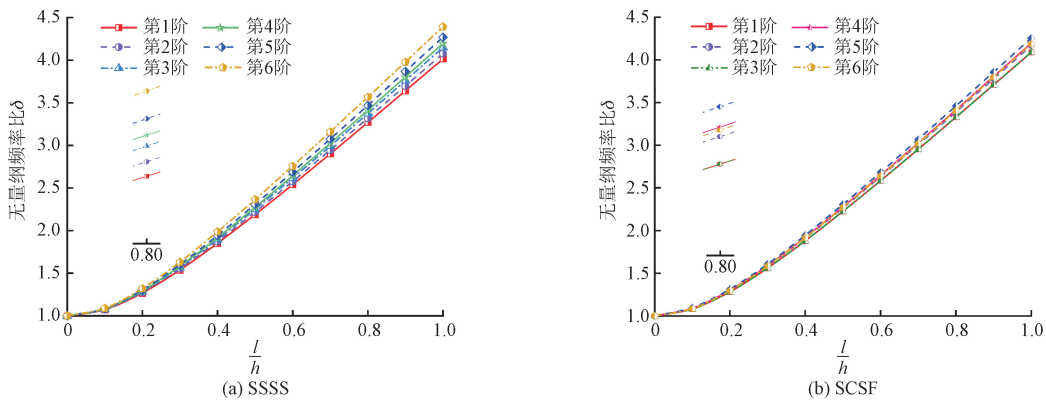

图 6　无量纲材料尺度参数对微板无量纲频率比的影响

Fig. 6　Influence of dimensionless material length-scale parameter on the dimensionless frequencies ratio of a microplate

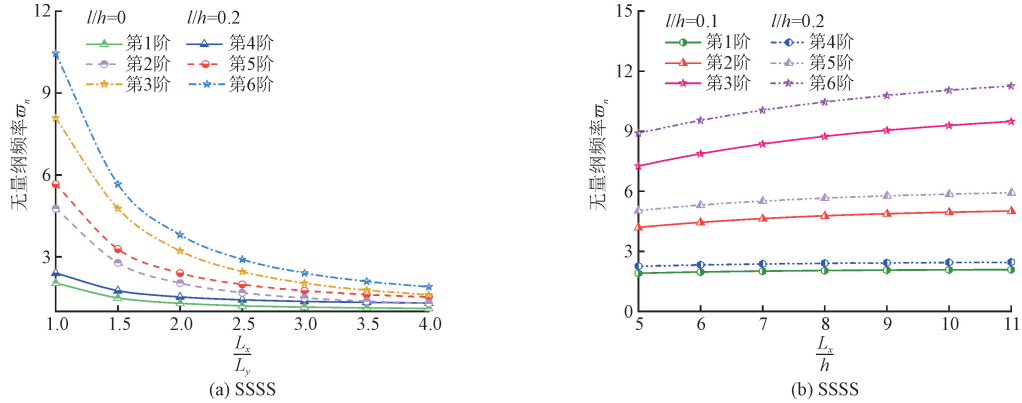

图 7 几何尺寸对微板无量纲频率的影响

Fig. 7 Influences of geometric sizes on the dimensionless frequencies of a microplate

为了量化尺度效应对微板各阶振动模态的影响程度,可以对 $l/h > 0$ 和 $l/h = 0$ 两种情形下对应模态向量进行相关性分析。第 i 阶模态向量的相关系数 R_i 定义如下

$$R_i = \left| \frac{n\ [\boldsymbol{X}_i]^{\mathrm{T}}\boldsymbol{Y}_i - n^2\ \overline{\boldsymbol{X}}_i\ \overline{\boldsymbol{Y}}_i}{\sqrt{[\boldsymbol{X}_i]^{\mathrm{T}}\boldsymbol{X}_i - n^2\ \overline{\boldsymbol{X}}_i^2}\cdot\sqrt{[\boldsymbol{Y}_i]^{\mathrm{T}}\boldsymbol{Y}_i - n^2\ \overline{\boldsymbol{Y}}_i^2}} \right| \tag{30}$$

式中,$\boldsymbol{X}_i$ 和 $\boldsymbol{Y}_i$ 分别为 $l/h > 0$ 和 $l/h = 0$ 情形下微板对应的第 i 阶模态向量,$\overline{\boldsymbol{X}}_i$ 和 $\overline{\boldsymbol{Y}}_i$ 为两者对应的均值。

表 3 和表 4 分别列出了连续边界(CCFF)和不连续边界(FC-CF-SF-FS)条件下微板的前 8 阶无量纲频率、模态振型以及相关系数。从表 3 可以看到,CCFF 微板的前 4 阶模态的相关性都很强,相应的模态等值线变化极小,因而尺度效应对微板前 4 阶模态的影响十分微弱;而第 5 阶至第 8 阶模态对应的相关系数逐渐减小,反映了尺度效应的影响逐渐增强,观察第 8 阶模态中可以明显看到板中部区域等值线发生了变化。从表 4 可以看出,尺度效应对 FC-CF-SF-FS 微板的第 1、4、6、7 阶模态的影响十分显著,对其余模态的影响比较弱,并且影响程度不符合高阶强于低阶的规律。对比表 3 和表 4 还可以发现,较之于 CCFF 微板,FC-CF-SF-FS 的相关系数明显更低,微板模态振型的尺度效应更加显著,其原因在于边界约束的不连续性会使应变梯度增强。

表 3 尺度效应对 CCFF 微板无量纲频率及模态的影响

Tab. 3 Influence of scale effect on the dimensionless frequencies and mode shapes of a microplate(CCFF)

l/h	无量纲频率及模态振型							
	ϖ_1	ϖ_2	ϖ_3	ϖ_4	ϖ_5	ϖ_6	ϖ_7	ϖ_8
0	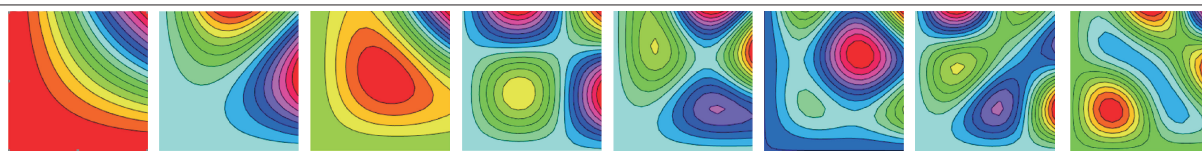							
	0.664 9	2.210 9	2.402 6	4.179 0	5.258 8	5.458 0	7.020 3	7.120 8
	1.000 0	1.000 0	1.000 0	1.000 0	1.000 0	1.000 0	1.000 0	1.000 0
0.5	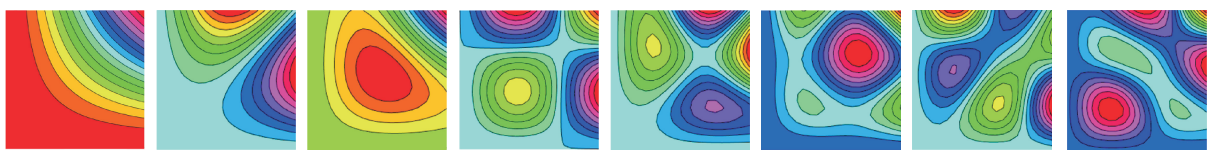							
	1.512 9	5.082 7	5.438 3	9.679 6	12.158 4	12.453 8	16.524 2	16.677 9
	0.999 9	0.999 6	0.999 2	0.999 0	0.998 1	0.996 1	0.987 2	0.985 7
1.0	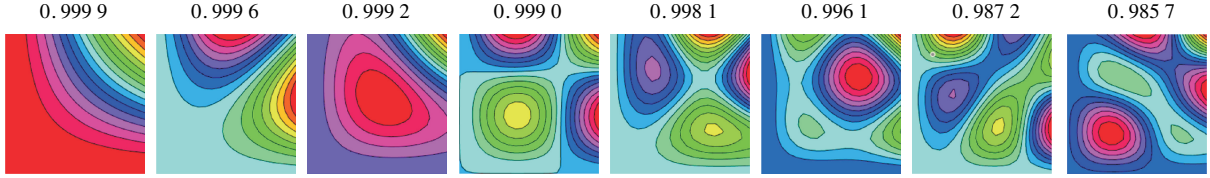							
	2.783 0	9.366 9	9.994 9	17.859 1	22.428 8	23.111 4	30.584 1	30.829 0
	0.999 9	0.999 6	0.999 1	0.998 9	0.997 8	0.995 5	0.982 7	0.981 0

表 4　尺度效应对 FC-CF-SF-FS 微板无量纲频率及模态的影响

Tab. 4　Influence of scale effect on the dimensionless frequencies and mode shapes of a microplate(FC-CF-SF-FS)

l/h	无量纲频率及模态振型							
	ϖ_1	ϖ_2	ϖ_3	ϖ_4	ϖ_5	ϖ_6	ϖ_7	ϖ_8
0		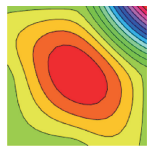		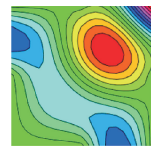	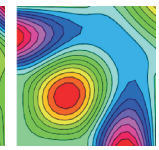	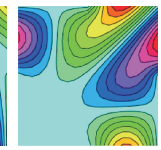	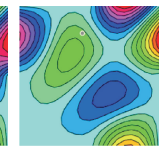	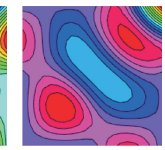
	1.919 1	2.357 5	3.986 2	4.929 7	5.384 9	6.410 2	7.300 5	7.768 9
	1.000 0	1.000 0	1.000 0	1.000 0	1.000 0	1.000 0	1.000 0	1.000 0
0.5			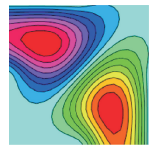	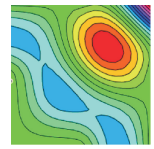	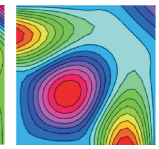	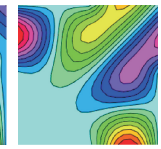	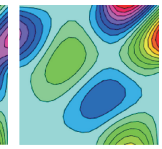	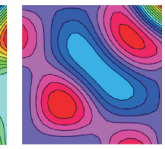
	4.643 2	5.550 2	9.347 1	11.466 1	12.584 0	15.433 8	17.613 4	18.287 1
	0.973 7	0.995 7	0.997 2	0.987 7	0.992 0	0.971 2	0.975 7	0.993 3
1.0			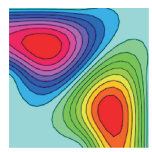	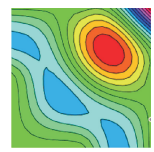	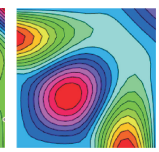	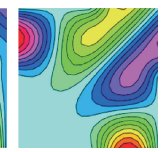	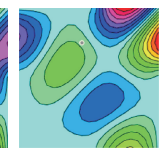	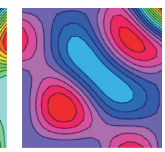
	8.579 8	10.247 6	17.219 5	21.162 7	23.213 4	28.570 4	32.682 7	33.807 3
	0.964 5	0.994 4	0.996 9	0.986 0	0.990 8	0.967 0	0.972 1	0.992 5

4　结　论

本研究将修正的应变梯度理论和精化高阶剪切变形理论相结合,发展了微尺度矩形厚板的自由振动模型。依次采用 Navier 法和微分求积有限元法获得了四边简支和一般边界条件下微板的自由振动频率。通过具体算例,验证了本研究模型的正确性,探讨了各因素对对微板振动频率及模态振型的影响,主要结论如下。

1)引入尺度效应会增强微板刚度,进而使微板各阶无量纲频率显著增大。

2)尺度效应对微板各阶无量纲频率的影响程度与边界条件、模态阶次、长宽比、长厚比有关。

3)较之于受连续边界约束的微板,受不连续边界约束的微板模态振型的尺度效应更加显著。

参考文献:

[1] 李贞坤, 程起有,冯志壮,等. 微尺度悬臂梁非线性振动实验研究与理论分析[J]. 实验力学,2021,36(6):793-803.
LI Zhenkun,CHENG Qiyou,FENG Zhizhuang,et al. Experimental and theoretical study on the nonlinear vibration of cantilever microbeams[J]. Journal of experimental mechanics,2021,36(6):793-803(in Chinese).

[2] LAM D C C,YANG F,CHONG A C M,et al. Experiments and theory in strain gradient elasticity[J]. Journal of the mechanics and physics of solids,2003,51(8):1477-1508.

[3] LI Z K,HE Y M,ZHANG B,et al. Experimental investigation and theoretical modelling on nonlinear dynamics of cantilevered microbeams[J]. European journal of mechanics-a/solids,2019,78:103834.

[4] LIU D B,HE Y M,TANG X T,et al. Size effects in the torsion of microscale copper wires:experiment and analysis[J]. Scripta materialia,2012,66(6):406-409.

[5] YANG F,CHONG A C M,LAM D C C,et al. Couple stress based strain gradient theory for elasticity[J]. International journal of solids and structures,2002,39(10):2731-2743.

[6] LIM C W,ZHANG G,REDDY J N. A higher-order nonlocal elasticity and strain gradient theory and its applications in wave propagation[J]. Journal of the mechanics and physics of solids,2015,78:298-313.

[7] 张立民,张波,张旭,等. 面内压缩荷载作用下双层微板系统的同步/异步屈曲[J]. 应用数学和力学,2023,44(2):160-167.
ZHANG Limin,ZHANG Bo,ZHANG Xu,et al. Synchronous/asynchronous buckling of double-layered microplate systems[J]. Applied mathematics and mechanics,2023,44(2):160-167(in Chinese).

[8] THAI H T,KIM S E. A simple higher-order shear deformation theory for bending and free vibration analysis of functionally graded plates[J]. Composite structures,2013,96:165-173.

[9] 马云龙,乔瑞,贺丹. 尺度依赖的静电驱动各向异性微板的

Pull-in 效应[J]. 应用力学学报,2020,37(3):1030-1035.
MA Yunlong, QIAO Rui, HE Dan. Size dependent Pull-in effect of electrostatically actuated anisotropic micro-plates[J]. Chinese journal of applied mechanics,2020,37(3):1030-1035(in Chinese).

[10] 王平,姚杰,王东贤. 四边简支载流纳米板的磁弹性稳定问题分析[J]. 应用力学学报,2020,37(5):1900-1906.
WANG Ping, YAO Jie, WANG Dongxian. Analysis of magneto-elastic stability of current-carrying nanoplates with four edges simply supported[J]. Chinese journal of applied mechanics, 2020, 37(5):1900-1906(in Chinese).

[11] 张振子,王平. 压电双层微板首次穿越问题研究[J]. 应用力学学报,2020,37(4):1696-1702.
ZHANG Zhenzi, WANG Ping. Study on the first passing problem of piezoelectric bilayer microplates[J]. Chinese journal of applied mechanics,2020,37(4):1696-1702(in Chinese).

[12] 王佳悦,王平. 微尺度载流纳米板在磁场中的磁弹性随机振动[J]. 应用力学学报,2023,40(5):1050-1057.
WANG Jiayue, WANG Ping. Magnetoelastic random vibration of micro-scale current-carrying nanoplates in a magnetic field[J]. Chinese journal of applied mechanics,2023,40(5):1050-1057(in Chinese).

[13] DUAN Y H, ZHANG B, LI X Y, et al. Size-dependent elastic buckling of two-variable refined microplates embedded in elastic medium[J]. International journal of applied mechanics,2022,14(4):2250039.

[14] DUAN Y H, ZHANG B, ZHANG X, et al. Accurate mechanical buckling analysis of couple stress-based skew thick microplates[J]. Aerospace science and technology,2023,132:108056.

[15] WEI L, QING H. Bending, buckling and vibration analysis of Bi-directional functionally graded circular/annular microplate based on MCST[J]. Composite structures,2022,292:115633.

[16] KARAMANLI A. Size-dependent behaviors of three directional functionally graded shear and normal deformable imperfect microplates[J]. Composite structures,2021,257:113076.

[17] ZHANG B, HE Y M, LIU D B, et al. A size-dependent third-order shear deformable plate model incorporating strain gradient effects for mechanical analysis of functionally graded circular/annular microplates[J]. Composites part b:engineering,2015,79:553-580.

[18] MIRSALEHI M, AZHARI M, AMOUSHAHI H. Buckling and free vibration of the FGM thin micro-plate based on the modified strain gradient theory and the spline finite strip method[J]. European journal of mechanics—a/solids,2017,61:1-13.

[19] TIMOSHIN A, KAZEMI A, BENI M H, et al. Nonlinear strain gradient forced vibration analysis of shear deformable microplates via Hermitian finite elements[J]. Thin-walled structures,2021,161:107515.

[20] ZHANG B, HE Y M, LIU D B, et al. An efficient size-dependent plate theory for bending, buckling and free vibration analyses of functionally graded microplates resting on elastic foundation[J]. Applied mathematical modelling,2015,39(13):3814-3845.

[21] THAI C H, FERREIRA A J M, PHUNG-VAN P. Free vibration analysis of functionally graded anisotropic microplates using modified strain gradient theory[J]. Engineering analysis with boundary elements,2020,117:284-298.

[22] KARAMANLI A, AYDOGDU M, VO T P. A comprehensive study on the size-dependent analysis of strain gradient multi-directional functionally graded microplates via finite element model[J]. Aerospace science and technology,2021,111:106550.

[23] KARAMANLI A, VO T P, CIVALEK O. Higher order finite element models for transient analysis of strain gradient functionally graded microplates[J]. European journal of mechanics—a/solids,2023,99:104933.

[24] HUNG P T, PHUNG-VAN P, THAI C H. A refined isogeometric plate analysis of porous metal foam microplates using modified strain gradient theory[J]. Composite structures, 2022, 289:115467.

[25] TANZADEH H, AMOUSHAHI H. Buckling analysis of orthotropic nanoplates based on nonlocal strain gradient theory using the higher-order finite strip method (H-FSM)[J]. European journal of mechanics—a/solids,2022,95:104622.

[26] CUONG-LE T, NGUYEN K D, HOANG-LE M, et al. Nonlocal strain gradient IGA numerical solution for static bending, free vibration and buckling of sigmoid FG sandwich nanoplate[J]. Physica B:condensed matter,2022,631:413726.

[27] 邹星,张波,张旭,等. 含尺度效应的功能梯度三明治微梁振动、弯曲与屈曲特性研究[J]. 固体力学学报,2022,43(3):344-359.
ZOU Xing, ZHANG Bo, ZHANG Xu, et al. Research on vibration, bending and buckling characteristics of functionally graded sandwich microbeams with size effects[J]. Chinese journal of solid mechanics,2022,43(3):344-359(in Chinese).

[28] ZHANG B, LI H, KONG L L, et al. Strain gradient differential quadrature beam finite elements[J]. Computers & structures, 2019,218:170-189.

[29] ZHANG B, LI H, KONG L L, et al. Strain gradient differential quadrature finite element for moderately thick micro-plates[J]. International journal for numerical methods in engineering,2020,121(24):5600-5646.

[30] ZHANG B, LI H, KONG L L, et al. Variational formulation and differential quadrature finite element for freely vibrating strain gradient Kirchhoff plates[J]. ZAMM-journal of applied mathematics and mechanics,2021,101(6):e202000046.

[31] ZHANG B, LI H, KONG L L, et al. Strain gradient differential quadrature Kirchhoff plate finite element with the C^2 partial compatibility[J]. European journal of mechanics—a/solids,2020,80:103879.

[32] ZHANG B, LI H, LIU J, et al. Surface energy-enriched gradient elastic Kirchhoff plate model and a novel weak-form solution scheme[J]. European journal of mechanics—a/solids,2021,85:104118.

(编辑 吕茵)

附录 A

$$\Sigma_1 = \frac{Gh^3}{12}\left(l_0^2+\frac{2l_1^2}{5}\right),\quad \Sigma_2 = \frac{Gh^3}{12}\left(l_0^2+\frac{12l_1^2}{5}\right),\quad \Sigma_3 = \frac{Gh^3}{252}\left(l_0^2+\frac{2l_1^2}{5}\right),$$

$$\Sigma_4 = \frac{Gh^3}{252}\left(l_0^2+\frac{12l_1^2}{5}\right),\quad \Sigma_5 = \frac{Gh^3}{30}\left(l_0^2+\frac{2l_1^2}{5}\right),\quad \Sigma_6 = \frac{Gh^3}{30}\left(l_0^2-\frac{3l_1^2}{5}\right),$$

$$\Sigma_7 = \frac{Gh^3}{6}\left(l_0^2-\frac{3l_1^2}{5}\right),\quad \Sigma_8 = \frac{Gh^3}{30}\left(l_0^2+\frac{12l_1^2}{5}\right),\quad \Sigma_9 = \frac{Gh^3}{126}\left(l_0^2-\frac{3l_1^2}{5}\right),$$

$$\Sigma_{10} = -\frac{4Ghl_1^2}{15},\quad \Sigma_{11} = \frac{Gh^3}{6}+2Gh\left(l_2^2+\frac{l_1^2}{3}\right),\quad \Sigma_{12} = \frac{14Gh}{15}\left(l_2^2+\frac{l_1^2}{3}\right)+\frac{Gh^3}{126},$$

$$\Sigma_{13} = \frac{D}{2}+Gh\left(\frac{4l_1^2}{15}+\frac{l_2^2}{2}+l_0^2\right),\quad \Sigma_{14} = \frac{D}{42}+\frac{Gh}{5}\left(l_0^2+\frac{28l_1^2}{45}+\frac{7l_2^2}{6}\right),$$

$$\Sigma_{15} = \frac{2Gh}{3}\left(\frac{l_1^2}{15}+l_0^2-l_2^2\right)+\frac{D\nu}{5},\quad \Sigma_{16} = \frac{2Gh}{3}\left(l_0^2+l_2^2-\frac{4l_1^2}{15}\right)+\frac{D}{5},$$

$$\Sigma_{17} = \frac{Gh}{5}\left(2l_0^2-\frac{7l_2^2}{3}-\frac{14l_1^2}{45}\right)+\frac{D\nu}{21},\quad \Sigma_{18} = Gh\left(2l_0^2-l_2^2-\frac{2l_1^2}{15}\right)+D\nu,$$

$$\Sigma_{19} = \frac{Gh^3}{15}+\frac{4Gh}{3}\left(2l_2^2-\frac{l_1^2}{3}\right),\quad \Sigma_{20} = \frac{4Gh}{15}+\frac{2G}{3h}\left(l_2^2+\frac{32l_1^2}{15}\right)$$